Computers in Biology and Medicine 168 (2024) 107747

Contents lists available at ScienceDirect

Computers in Biology and Medicine

journal homepage: www.elsevier.com/locate/compbiomed

Regularity and variability of functional brain connectivity characteristics between gyri and sulci under naturalistic stimulus

Zhenxiang Xiao [a], Liang He [a], Boyu Zhao [a], Mingxin Jiang [a], Wei Mao [a], Yuzhong Chen [a], Tuo Zhang [c], Xintao Hu [c], Tianming Liu [b], Xi Jiang [a,*]

[a] The Clinical Hospital of Chengdu Brain Science Institute, MOE Key Laboratory for NeuroInformation, School of Life Science and Technology, University of Electronic Science and Technology of China, 611731, Chengdu, Sichuan, China
[b] School of Computing, University of Georgia, 30602, Athens, USA
[c] School of Automation, Northwestern Polytechnical University, 710129, Xi'an, China

ARTICLE INFO

Keywords:
Functional connectivity
Naturalistic stimulus
7T functional magnetic resonance imaging
Spatio-temporal graph convolutional networks
Gyri and sulci

ABSTRACT

The human cerebral cortex is folded into two fundamentally anatomical units: gyri and sulci. Previous studies have demonstrated the genetical, structural, and functional differences between gyri and sulci, providing a unique perspective for revealing the relationship among brain function, cognition, and behavior. While previous studies mainly focus on the functional differences between gyri and sulci under resting or task-evoked state, such characteristics under naturalistic stimulus (NS) which reflects real-world dynamic environments are largely unknown. To address this question, this study systematically investigates spatio-temporal functional connectivity (FC) characteristics between gyri and sulci under NS using a spatio-temporal graph convolutional network model. Based on the public Human Connectome Project dataset of 174 subjects with four different runs of both movie-watching NS and resting state 7T functional MRI data, we successfully identify unique FC features under NS, which are mainly involved in visual, auditory, emotional and cognitive control, and achieve high discriminative accuracy 93.06 % to resting state. Moreover, gyral regions as well as gyro-gyral connections consistently participate more as functional information exchange hubs than sulcal ones among these networks. This study provides novel insights into the functional brain mechanism under NS and lays a solid foundation for accurately mapping the brain anatomy-function relationship.

1. Introduction

The highly folded cerebral cortex is one of the most essential features of human brain, consisting of functionally protruding gyri and depressed sulci [1–4] that constitute the biological basis of higher-order brain functions [5]. Gyri and sulci exhibit significant differences in genetics [6], morphology [7], anatomy [8], axonal connections [9], and functions [10] and can be regarded as two fundamental functional units of the brain anatomy [11], providing a unique perspective for characterizing the relationship among brain function, cognition, and behavior [12,13].

Functional Magnetic Resonance Imaging (fMRI) data with high spatio-temporal resolution has been widely used for probing the functional characteristics between gyri and sulci. Combining it with sophisticated computational models, some pioneering studies have identified significant functional differences between gyri and sulci as well as their associations with cognitive behavior [10,11,14,15]. Specifically, compared to sulcal fMRI BOLD signals with more complex and high-frequency temporal patterns, the gyral ones concentrate more on low-frequency band under both resting and task-evoked states across different species such as humans and macaques [10,11,16]. Compared to sulco-sulcal functional connectivity, the gyro-gyral ones are more involved in long-range with stronger strength within the brain network [2,14,17]. Such functional difference between gyri and sulci are related to fluid intelligence [15], crystal intelligence, and spatial orientation across multiple task-evoke conditions [14]. These findings have suggested different functional roles between gyri and sulci in cognitive performances, i.e., gyri may serve as global functional information exchange hubs while sulci act as the local functional information processing units [2].

Although these studies have provided unique perspectives in exploring functional differences between gyri and sulci under resting or

* Corresponding author.
E-mail address: xijiang@uestc.edu.cn (X. Jiang).

https://doi.org/10.1016/j.compbiomed.2023.107747
Received 7 August 2023; Received in revised form 5 November 2023; Accepted 20 November 2023
Available online 23 November 2023

task-evoked state, such characteristics under naturalistic stimulus which reflects real-world dynamic environments are largely unknown. People are often in a more dynamic natural environment in their daily lives and constantly receiving complex and diverse natural stimuli such as touch, hearing, and vision, requiring the brain to simultaneously process such multi-model information [18–21]. Compared to the resting state or specific task stimuli, the naturalistic stimuli can simultaneously evoke complex brain functions consisting of a wide range of brain networks and regions [21–25]. Therefore, it is crucial to investigate the functional brain connectivity characteristics between gyri and sulci under naturalistic stimulus in order to provide a more accurate mapping between brain anatomy and function.

In order to address this question, this study systematically investigates the regularity and variability of gyro-sulcal functional connectivity characteristics under naturalistic stimulus using a spatio-temporal graph convolutional network model. Graph convolutional networks [26] represent complex spatial topological structure of graphs and have received increasing interest in modeling brain networks as graphs in recent years. Among various graph models, the spatio-temporal graph convolutional network (ST-GCN) can fully integrate the four-dimensional spatio-temporal information of fMRI data to detect the dynamic changes in time as well as the inherent spatial functional connectivity patterns [27–29]. Specifically, we first construct the spatio-temporal graph based on the functional connectivity matrices among gyral/sulcal brain regions. We then feed the constructed graphs into the ST-GCN model to identify unique functional connectivity features under the naturalistic stimulus compared to resting state as a baseline. We finally investigate the inherent regularity and variability of functional connectivity between gyri and sulci from the identified unique functional connectivity features.

We evaluate the proposed framework on 7T fMRI data of 174 healthy adults from the publicly available Human Connectome Project (HCP). We perform extensive classification performance comparisons of ST-GCN with other baseline models across four different runs of naturalistic stimulus and resting state fMRI data. We hypothesize that compared to other models, our proposed framework can more accurately identify unique functional connectivity features under the naturalistic stimulus which has higher classification accuracy with those under the resting state. We also hypothesize that gyri and sulci may play different functional roles in terms of different number of regions and connections within the functional connectivity features to encode the cognitive brain function under naturalistic stimulus.

The major novelties and contributions of our study are as follows.

(1) Our study is one of the earliest studies on the functional connectivity characteristics difference between gyri and sulci under naturalistic stimulus (NS) using 7T functional MRI data.
(2) We adopt a spatio-temporal graph convolutional network (ST-GCN) to identify unique functional connectivity features which achieve the highest classification performance compared with other baseline models. The extracted functional connectivity features exhibit regularity in terms of functional interactions both within and among auditory, visual, emotional, and cognitive control networks.
(3) Our study identifies that gyral regions and gyro-gyral connections consistently participate more than sulcal regions and sulco-sulcal connections, suggesting that gyri are global functional information exchange hubs and sulci are local functional information processing units under naturalistic stimulus, which lays a solid foundation for accurately mapping between brain anatomy and function.

2. Material and methods

2.1. Data acquisition and preprocessing

This study uses the public 7T fMRI data from the Human Connectome Project (HCP) [30] with approval. All 174 subjects including 69 males and 105 females (29.34 ± 3.28 years old) with complete fMRI data are included in the study. Each subject is scanned under four resting states (i.e., REST1-REST4) as well as movie-watching states (i.e., MOVIE1-MOVIE4). During the resting state scan, subjects remain relaxed and eyes open to look at the screen with a bright crosshair on dark background. All resting state runs have a fixed scan time of 900s. During the movie-watching scan, subjects watch 4 or 5 different movie clips of freely available independent films under Creative Commons licensing or from Hollywood movies whose duration vary from 63s to 259s. The total scan time of the four movie-watching runs ranges from 901s to 921s. More details about the scanning protocol and movie contents are in https://www.humanconnectome.org/hcp-protocols-ya-7t-imaging. The major acquisition parameters of fMRI are: matrix = 130 × 130, FOV = 208 × 208 mm^2, slice thickness = 1.6 mm, number of slices = 85, TR = 1000 ms, TE = 22.2 ms, and flip angle = 45°.

The format of the fMRI data we obtained in the study is CIFTI, which consists of GIFTI surface data and NIFTI volume data [31]. The commonly used HCP minimal preprocessing pipeline is adopted for the data preprocessing including two major steps of fMRIVolume and fMRISurface [31]. At the fMRIVolume step, spatial distortion removal, motion correction, registration to the structure image, bias correction, and global normalization are performed. Specifically, we first perform the gradient-nonlinearity-induced distortion correction, then realign the time series to correct for subject motion, and finally concatenate all of the transforms for each correction into a single transformation. At the fMRISurface step, the fMRI data in voxel space are registered and mapped onto the cortical surface grid of high-resolution Conte 69 mesh [31]. Additionally, we cut off the last few frames of each movie-watching scan to ensure consistent scan time of 900s with the resting state for fair comparisons.

2.2. Construction of spatio-temporal graph based on functional connectivity

We first define the gyral/sulcal brain regions based on the Desikan-Killiany atlas (DK atlas) and "sulc" value information [32,33] of the cortical surface (Fig. 1a). The DK atlas divides the cortical surface into 68 regions of interest (ROIs) and the "sulc" value of a cortical vertex measures average convexity signing the movement of the cortical development process [11,32,34]. For each ROI in DK atlas, we sort all cortical vertices within the ROI based on the "sulc" values and define top 20 % vertices with largest 'sulc' values as gyri and bottom 20 % ones with smallest 'sulc' values as sulci [15]. We therefore obtain a finer-scale DK atlas (i.e., GSDK atlas) containing 136 ROIs with 68 gyral and 68 sulcal regions. The averaged fMRI BOLD signal of each gyral/sulcal ROI is calculated based on all BOLD signals of vertices within the ROI.

We then define edge and node features of the spatio-temporal graph based on the gyral/sulcal ROIs (Fig. 1b). Note that in this study, we focus on the functional connectivity which quantifies the fMRI BOLD signal synchrony between two brain ROIs. The effective connectivity which measures the causal influence of one ROI's functional activity on another one is left for future studies. Specifically, for the edge feature, we calculate functional connectivity as the widely adopted Pearson's correlation coefficient $\dot{c}_{ij} = \frac{cov(S_i,S_j)}{\sigma_{S_i}\sigma_{S_j}}$ of two fMRI BOLD signals S_i and S_j between any pair of gyral/sulcal ROIs i and j, where $cov(\bullet)$ is the covariance, σ_{S_i} and σ_{S_j} are the standard deviations of the signals. The spatial edge feature is therefore denoted as $E_{Spatial} = \{\dot{c}_{i,j} | i, j = 1, 2, \ldots, 136 \; and \; i \neq j\}$. For the node feature, a fixed time window is adopted to

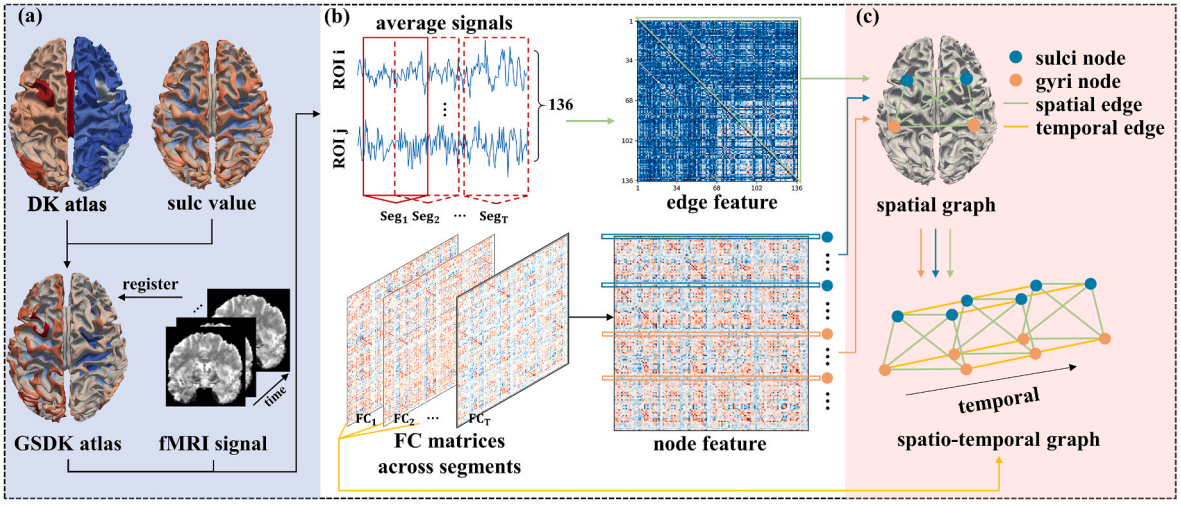

Fig. 1. Pipeline of constructing spatio-temporal graph based on gyro-sulcal functional connectivity. (a) Definition of the gyral/sulcal brain regions based on the DK atlas and "sulc" value information to obtain a finer-scale GSDK atlas of 136 gyral/sulcal ROIs and the associated fMRI signal; (b) Definition of edge and node features of the spatio-temporal graph based on the gyral/sulcal ROIs; (c) Construction of the spatio-temporal graph based on the defined edge and node features.

equally divide the time series of BOLD signals into T segments, and the functional connectivity matrix among all ROIs is calculated within each segment, respectively. After that, the degree of i-th ROI at the t-th segment is calculated as the node feature $v_i^{(t)} = \sum_{i \neq j} c_{ij}^{(t)}$, where $c_{ij}^{(t)}$ is the functional connectivity value between ROI i and ROI j at the t-th segment [2,35].

We finally construct the spatio-temporal graph based on the defined edge and node features (Fig. 1c). The spatial graph $G^{(t)}$ at t-th segment is constructed based on the spatial edge feature $E_{Spatial}$ and the set of node features $V^{(t)} = \{v_i^{(t)} | i = 1, 2, \ldots, 136\}$, where $t = 1, 2, \ldots, T$. The corresponding ROIs of spatial graphs $G^{(t)}$ between any two adjacent segments are then concatenated by the temporal edge $E_{Temporal} = \{c_i^{t,t+1} = 1 | t = 1, 2, \ldots, T-1; i = 1, 2, \ldots, 136\}$ to obtain the spatio-temporal graph G.

2.3. Identification of unique functional connectivity under naturalistic stimulus

We feed the constructed spatio-temporal graphs under both naturalistic stimulus and resting state into the ST-GCN classification model in order to identify the unique functional connectivity features under the naturalistic stimulus compared to the baseline resting state (Fig. 2a). The major modules of ST-GCN are shown in Fig. 2b, including a batch normalization (BN) layer, a spatial graph convolutional network (SGCN), a temporal convolutional network (TCN), a global average pooling (GAP) layer, and a fully connected layer (FCL). Firstly, we input the constructed spatio-temporal graphs as f_{in} with a BN operation to reduce the internal covariate shift among different subjects in the same batch [36], and the output is denoted as $f_{in}^{'}$. Secondly, we carry out a graph convolution on the spatial graph $G^{(t)}$ with a spatial convolutional kernel W_{SG} for each segment similar to SGCN [28]. The output $f_s^{'}$ is calculated by:

$$f_s^{'} = \Lambda^{-\frac{1}{2}}((A + I) \otimes M)\Lambda^{-\frac{1}{2}} f_{in}^{'} W_{SG} \tag{1}$$

where $A \in R^{136 \times 136}$ is the spatial edge feature matrix, I is an identity matrix, Λ is defined as $\Lambda^{ii} = \sum_j A^{ij} + I^{ii}$, and $\otimes$ represents the element-wise product operation. Notably, a learnable edge weight matrix $M \in R^{136 \times 136}$ is introduced to the spatial edge feature in Eq. (1). The initialized all-one matrix M reduces gradually during the training of model, in which the edges representing unique functional connectivity and thus contributing to classification also drop more slowly. Thirdly, the TCN with a temporal convolutional kernel W_T is calculated at the temporal level by performing 1D convolution operation for each ROI at the time series respectively. The output $f_t^{'}$ of the temporal convolution is:

$$f_t^{'} = ReLU(f_s^{'} \circledast W_T) \tag{2}$$

where $\circledast$ denotes the convolution, $ReLU$ denotes the ReLU activation function [37]. Finally, the output classification label is obtained after the GAP and FCL [38] together with the edge weight matrix M representing unique functional connectivity features under naturalistic stimulus compared to the baseline resting state for the subsequent analysis.

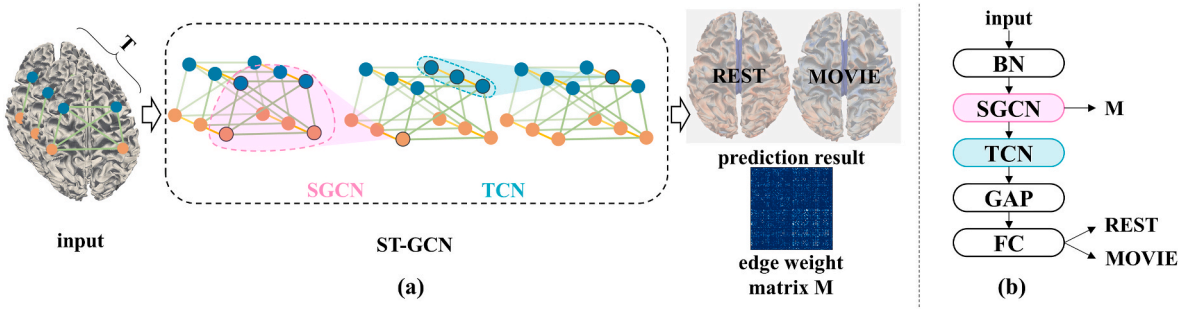

Fig. 2. Identification of unique functional connectivity features under the naturalistic stimulus compared to the baseline resting state. (a) Overview of the ST-GCN classification model; (b) The major modules of ST-GCN.

2.4. Identification of functional connectivity regularity and variability between gyri and sulci

We further investigate the regularity and variability of functional connectivity between gyri and sulci from the identified unique functional connectivity features M. Firstly, in order to obtain stable and accurate features across different subjects and experiment runs, we repeat the model training 100 times using one run as training set and the other three runs as the test set. After sorting all values of the upper triangular matrix of M and obtaining 100 ranks of each functional connectivity across 100 times, one-sample t-test is performed for each connectivity with a threshold k and false discovery rate (FDR) correction to obtain stable functional connectivity features M. The reproducibility of different thresholds k is reported in Section 3.2. Secondly, each functional connectivity in M is categorized into G-G, G-S, and S–S types corresponding to functional connectivity between gyro-gyral, gyro-sulcal, and sulco-sulcal ROIs, and further normalized for fair comparison:

$$\boldsymbol{P} = \begin{cases} \dfrac{2\boldsymbol{C}_{G-G}}{\boldsymbol{N}_G(\boldsymbol{N}_G - \mathbf{1})} & \text{in } \mathbf{G\text{-}G} \text{ type} \\ \dfrac{\boldsymbol{C}_{G-S}}{\boldsymbol{N}_G\boldsymbol{N}_S} & \text{in } \mathbf{G\text{-}S} \text{ type} \\ \dfrac{2\boldsymbol{C}_{S-S}}{\boldsymbol{N}_S(\boldsymbol{N}_S - \mathbf{1})} & \text{in } \mathbf{S\text{-}S} \text{ type} \end{cases} \tag{3}$$

where $\boldsymbol{C}_{G-G}$, $\boldsymbol{C}_{G-S}$, and $\boldsymbol{C}_{S-S}$ are the number of connections in G-G, G-S, and S–S type, respectively. N_G and N_S are the number of gyral and sulcal ROIs, respectively. The quantitative comparisons of the number of three types (G-G, G-S, and S–S) as well as the number of two types of ROIs (gyral and sulcal) are performed to investigate the regularity and variability of functional connectivity characteristics between gyri and sulci under movie-watching naturalistic stimulation.

2.5. Model training scheme and parameter setting

We adopt 5-fold cross-validation strategy which is widely used in previous studies [39] to ensure the robustness of the classification results. In our study, all subjects are split into 140 as the training set and 34 as the test set in each fold, respectively. We use the BCELoss as the loss function and employ the Adam optimizer with default betas of 0.9 and 0.999 [40]. We set the learning rate to 0.001 with a decay rate weight of 0.0001, the dropout rate as 0.5 to reduce the overfitting, the batch size to 32, the total quantity of epochs to 300, and the temporal kernel size to 9. The model training is based on the Pytorch framework with a GTX3090 GPU.

2.6. Performance metrics of the model

In this study, we use several metrics including Confusion Matrix, Accuracy, Sensitivity, Specificity and F1 Score to evaluate the model performance. As shown in Fig. 3a, the Confusion Matrix divides all samples into four categories based on the real labels and predicted results: True Positive (TP), True Negative (TN), False Positive (FP), and False Negative (FN) [41].

Accuracy measures the overall prediction accuracy of the classifier, and is defined as the proportion of the number of samples correctly predicted by the model to the total number of samples:

$$\boldsymbol{Accuracy} = \frac{\mathrm{TP} + \mathrm{TN}}{\mathrm{TP} + \mathrm{TN} + \mathrm{FP} + \mathrm{FN}} \tag{4}$$

Sensitivity, also known as True Positive Rate or Recall, refers to the proportion of the number of positive samples correctly predicted by the model to the total number of positive samples:

$$\boldsymbol{Sensitivity} = \frac{\mathrm{TP}}{\mathrm{TP} + \mathrm{FN}} \tag{5}$$

Specificity, which measures the ability to identify negative samples, refers to the proportion of the number of negative examples correctly predicted by the model to the total number of negative samples:

$$\boldsymbol{Specificity} = \frac{\mathrm{TN}}{\mathrm{TN} + \mathrm{FP}} \tag{6}$$

F1 Score is a comprehensive evaluation index that combines Accuracy and Recall to measure the precision and recall capabilities of a classifier:

$$\boldsymbol{F1\ Score} = \frac{2 * \mathrm{Accuracy} * \mathrm{Sensitivity}}{\mathrm{Accuracy} + \mathrm{Sensitivity}} \tag{7}$$

3. Results and discussion

3.1. Classification performance of unique functional connectivity features

We evaluate the model's ability to identify the unique functional connectivity features under the naturalistic stimulus by comparing the classification performance metrics including accuracy, sensitivity, specificity, and F1 score between naturalistic stimulus and resting state across different models. The rationale is that more accurately identified unique functional connectivity features under naturalistic stimulus would have better performance in classification with those under resting state as the baseline. We compare the classification performance of the proposed ST-GCN with four representative baseline models including Support Vector Machine (SVM), 1D-CNN, Long Short Term Memory (LSTM), and CNN + LSTM, as well as three different model architectures including TCN only, SGCN only, and ST-GCN without M as ablation studies. As reported in Table 1, the proposed ST-GCN achieves highest performance in all metrics with 93.06 % averaged accuracy, 93.75 % averaged sensitivity, 92.39 % averaged specificity and 93.10 % averaged F1 score across all four runs of data compared to other baseline models as well as other model architectures. The detailed values of sensitivity, specificity and F1 score in each run are reported in Supplemental Tables 1–3, respectively. We further report the sum of the confusion matrices across the five folds in each run (Fig. 3b-e), which consistently indicates the discriminative capacity of our model in distinguishing the movie-watching state from the resting state.

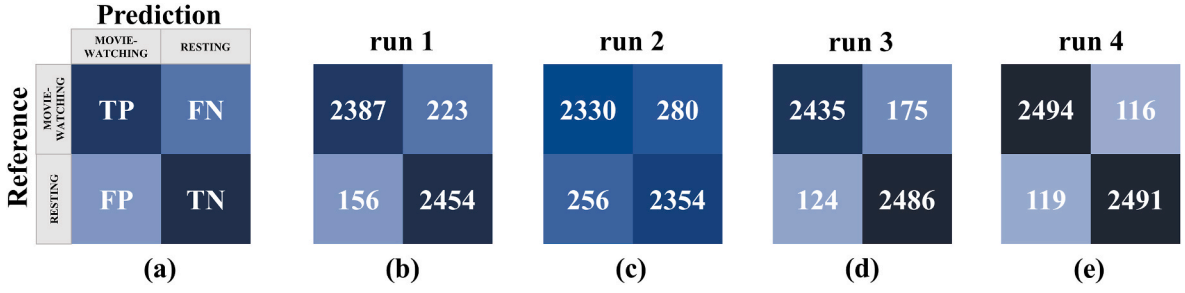

Fig. 3. Visualization of the Confusion Matrix. (a) The composition of the Confusion Matrix. (b–e) The Confusion Matrix in each of the four runs.

Table 1
Classification performance (%) of different models and architectures in 5-fold cross-validation. The data is represented as mean ± std.

	Model	Accuracy					Sensitivity	Specificity	F1 Score
		run 1	run 2	run 3	run 4	Average	Average	Average	Average
Baseline	SVM	65.11 ± 1.22	63.37 ± 1.86	54.92 ± 0.97	64.89 ± 1.32	62.07 ± 4.40	91.41 + 2.28	32.74 + 9.03	70.75 + 2.41
	1D-CNN	81.21 + 1.01	85.77 + 1.25	86.53 + 0.56	84.73 + 1.26	84.56 + 2.30	83.75 + 5.41	85.37 + 5.12	84.39 + 2.50
	LSTM	84.31 ± 3.14	85.98 ± 3.09	86.37 ± 2.09	86.57 ± 4.07	85.81 ± 3.14	89.31 + 4.99	81.43 + 7.92	85.96 + 2.91
	CNN + LSTM	90.03 ± 3.21	89.26 ± 3.23	87.75 ± 3.73	90.95 ± 3.20	89.47 ± 3.56	92.57 + 4.41	86.81 + 5.11	89.97 + 1.37
Ablation Study	TCN	59.50 ± 1.86	64.81 + 1.43	67.82 + 1.03	59.20 + 0.48	62.83 + 3.87	62.22 + 4.67	63.44 + 6.50	62.59 + 3.75
	SGCN	76.57 + 1.13	74.04 + 0.50	90.77 + 0.44	79.73 + 0.20	80.28 + 6.42	79.64 + 8.71	80.92 + 4.34	80.00 + 6.78
	ST-GCN W/o M	84.87 ± 9.68	84.62 ± 10.17	92.82 ± 0.72	93.85 ± 1.31	89.04 ± 8.27	90.89 + 8.50	87.06 + 9.09	89.20 + 8.12
Proposed	**ST-GCN**	**92.74 ± 0.80**	**89.71 ± 3.09**	**94.27 ± 0.73**	**95.50 ± 0.92**	**93.06 ± 2.75**	**93.75 + 3.21**	**92.39 + 3.02**	**93.10 + 2.77**

In summary, the proposed model can not only effectively characterize the functional connectivity features among gyral/sulcal regions, but also accurately identify unique functional connectivity features under naturalistic stimulus compared to resting state.

3.2. Regularity and variability of unique functional connectivity features

We demonstrate regularity and variability of the unique functional connectivity features. Fig. 4 shows the functional connectivity features in run 4 as an example derived from different threshold values (0.2 %–1.2 %, and 0.2 % as the interval) of k in M as detailed in Section 2.4. We see that the overall pattern distribution of functional connectivity features is relatively stable across a specific range of threshold values (0.6–1.2), suggesting the robustness of identified functional connectivity features. Specifically, the involved functional connections are mainly among cuneus, fusiform, superior temporal, and transverse temporal gyri which are part of visual and auditory networks [42,43], as well as frontal lobe and limbic regions which are related to emotional and cognitive control [44,45].

We then visualize the unique functional connectivity features across all four runs. Fig. 5a shows the whole-brain functional connectivity features that exist in at least two out four runs when $k = 5$ %. We see that there are common functional connections across most of the four runs including 1) right pars triangularis sulcus with right insula sulcus, 2) right transverse temporal gyrus with right superior frontal sulcus, 3) right transverse temporal gyrus with left transverse temporal sulcus, 4) left postcentral gyrus with left transverse temporal gyrus, 5) left precentral gyrus with left transverse temporal gyrus, 6) left precentral gyrus with left superior temporal gyrus, and 7) left postcentral gyrus with left superior parietal gyrus. Among them, left transverse temporal gyrus, which belongs to the primary auditory cortex and is activated by musical stimulation [46,47], has the most connections to the other regions. The superior temporal gyrus and right transverse temporal gyrus which are associated with auditory tasks [46,47] also have more connections with other regions. Fig. 5d further visualizes the degree of involved brain regions of the functional connectivity features. The top five regions that are mostly involved in these functional connectivity features are right and left transverse temporal gyrus, left supramarginal gyrus, right cuneus sulcus, and left pericalcarine gyri. which are highly correlated with the auditory system and visual system [48–51]. We further divide the whole-brain functional connectivity features across four runs into inter-hemispheric and intra-hemispheric ones, respectively as shown in Fig. 5b–c. The degree of involved brain regions of the inter- and intra-hemispheric features is also visualized in Fig. 5e–f. We see that the auditory functional networks such as transverse temporal lobe are involved in both inter- and intra-hemispheric functions. However, the inter-hemispheric connections also involve visual networks such as cuneus as well as emotional and cognitive control networks such as frontal lobe, while the intra-hemispheric ones involve more regions of auditory function such as superior temporal gyrus [48,51].

In summary, although there are certain variabilities of unique functional connectivity features across the four runs since the detailed contents of movie-watching stimulus are different, there are still functional connectivity regularity in terms of functional interactions within and among auditory, visual, emotional, and cognitive control networks during naturalistic stimulus.

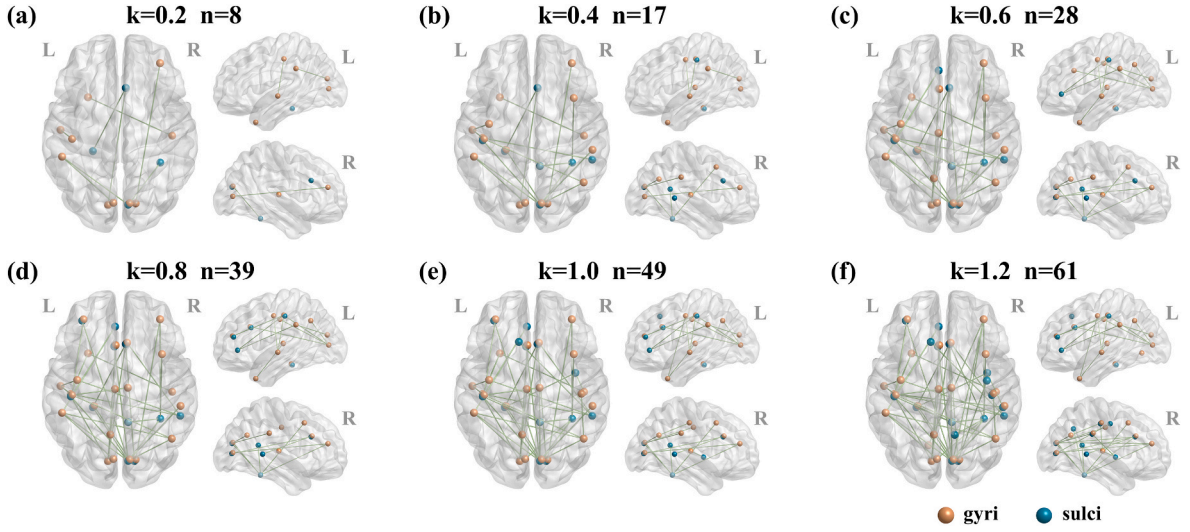

Fig. 4. Visualization of the gyro-sulcal functional connectivity pattern within run 4 as an example derived from six different threshold values (0.2 %–1.2 %, and 0.2 % as the interval) of k. (a)–(f) show the connectivity pattern under each of the six threshold values, respectively. In each sub-figure, n is the number of significant connections after FDR correction. Orange and blue spheres represent gyral and sulcal regions, respectively. The green lines represent the connections.

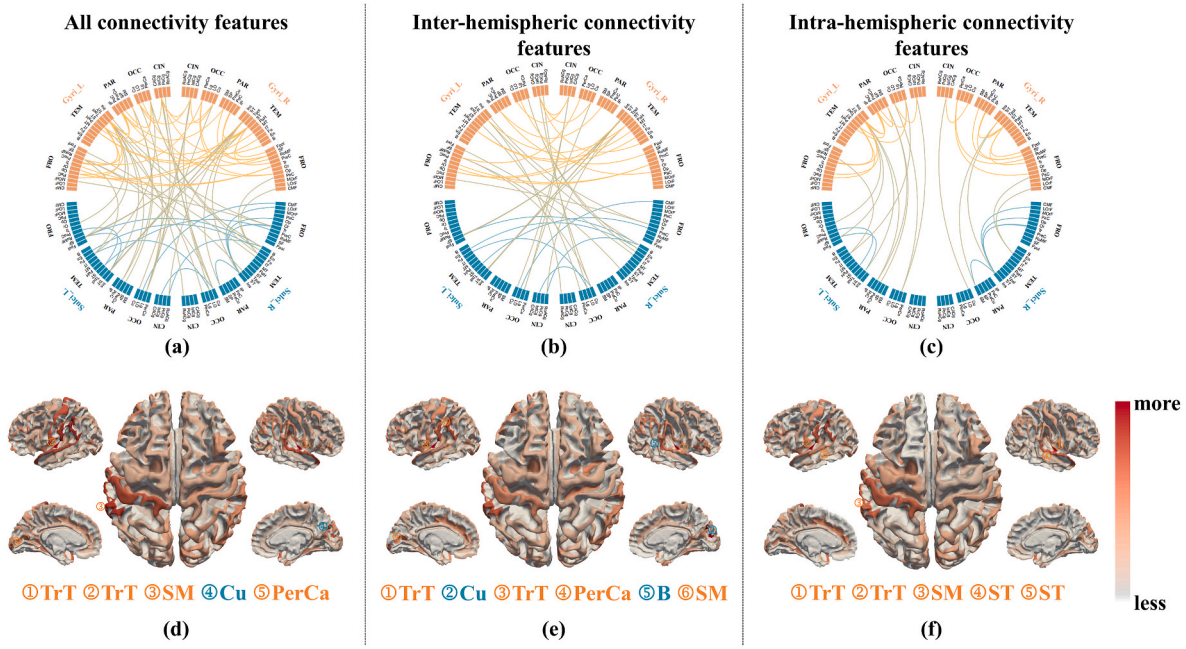

Fig. 5. The unique functional connectivity features across all four runs at whole-brain, inter-hemisphere and intra-hemisphere. (a–c) show the circle plot of the unique functional connectivity features that exist in at least two out four runs when $k = 5$ %. The gold, green and cyan curves represent G-G, G-S, and S–S connections, respectively. Thicker curves indicate existence in more runs. (d–f) show the degree of involved brain regions of the functional connectivity features. The names of top five regions that are mostly involved in the functional connectivity features are provided. Orange and blue fonts indicate gyral and sulcal regions, respectively. CIN: cingulate cortex; OCC: occipital lobe; PAR: parietal lobe; TEM: temporal lobe; FRP: frontal lobe; TrT: transverse temporal; SM: supramarginal; Cu: cuneus; PerCa: pericalcarine; ST: Superior temporal; B: bankssts.

3.3. *Functional connectivity characteristics differences between gyri and sulci*

We further investigate the functional connectivity characteristics difference between gyri and sulci within the unique functional connectivity pattern. Fig. 6 visualizes the unique functional connectivity pattern when $k = 0.6$ % as an example within all four runs. In run 1 (Fig. 6a), the functional connections are mainly among fusiform, lateral occipital, pericalcarine, lingual, temporal lobe, and superior frontal regions, which are involved in visual, auditory, and face recognition

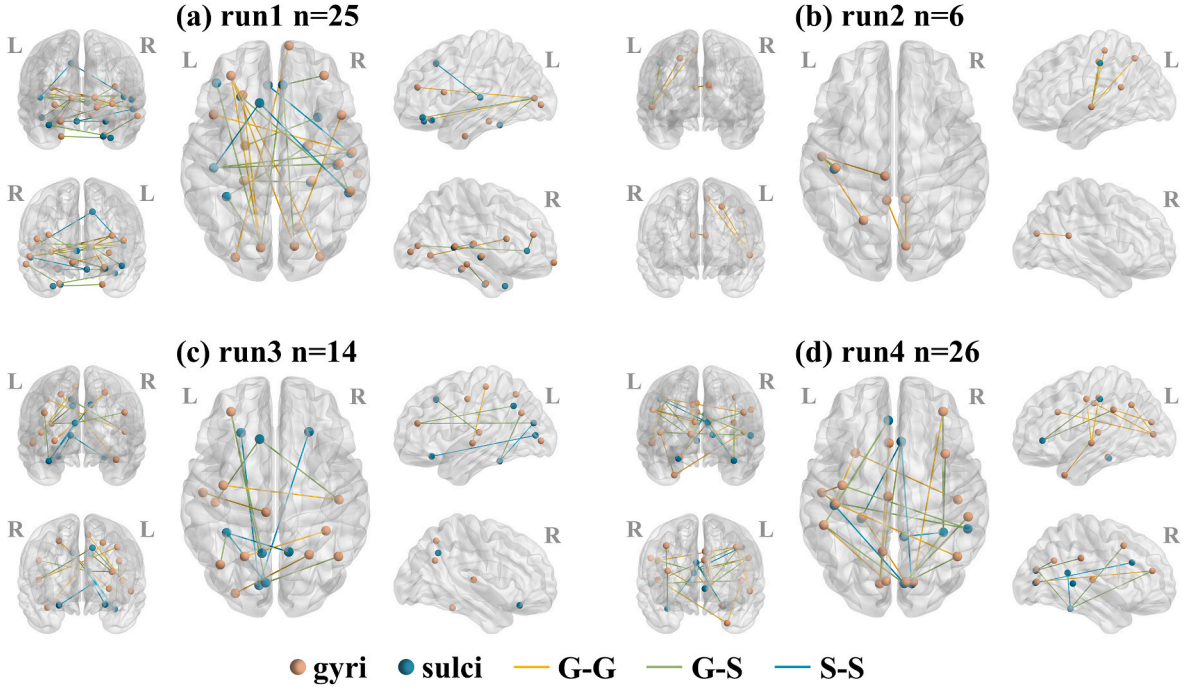

Fig. 6. Visualization of the gyro-sulcal functional connectivity pattern within all four runs when $k = 0.6$ % as an example. (a)–(d) show the connectivity pattern within each of the four runs, respectively. In each sub-figure, n is the number of significant connections after FDR correction. Orange and blue spheres represent gyral and sulcal regions, respectively. The gold, green and cyan lines represent G-G, G-S, and S–S connections, respectively.

functions [52–54]. In run 2 (Fig. 6b), the total number of connections is less than run 1 from visual inspection, while the superior temporal region and cuneus are major hubs connecting with other regions. The superior temporal region is more active when listening to the sound of the sentence than environmental sounds stimuli [46], and the cuneus is the central cortical hub of visual networks [43]. In run 3 (Fig. 6c), the connections are also among occipital and temporal lobes, as well as superior frontal regions which are similar to run 1. In run 4 (Fig. 6d), the connections are mainly among visual and auditory networks [42,43] including cuneus, fusiform, superior temporal region and transverse temporal gyri, as well as emotional and cognitive control networks [44,45] including frontal lobe and limbic structure.

Although Fig. 6 illustrates the considerable variability of the functional connectivity pattern among the four runs due to different contents of movie-watching stimulus, we identify consistent functional connectivity characteristics difference between gyri and sulci within those patterns. From visual inspection, the involved number of gyral nodes as well as gyro-gyral connections is consistently more than sulcal nodes and sulco-sulcal connections, respectively across the four runs. Quantitatively, a paired *t*-test ($p < 0.05$) is conducted to compare the percentage of involved numbers between gyral and sulcal nodes when k ranges from 0.2 % to 5 % (0.2 % as the interval). We see that the percentage of number of gyral nodes (mean value of 70.8 %, 34.6 %, 45.2 % and 49.1 %) is significantly higher than that of sulcal nodes (mean percentage of 52.4 %, 32.8 %, 41.1 % and 40.7 %) in each of the four runs (Fig. 7). We further compare the percentage of numbers among gyro-gyral (G-G), gyro-sulcal (G-S), and sulco-sulcal (S–S) connections using one-way ANOVA ($p < 0.05$) and post-hoc t-tests ($p < 0.05$, Bonferroni correction for multiple comparisons). There is significant difference among the three types of connections in each of the four runs as reported in Table 2. Moreover, the percentage of number of G-G connections (mean value of 2.64 %, 0.85 %, 1.36 % and 2.12 %) is significantly larger than that of G-S (mean value of 1.49 %, 0.60 %, 0.79 % and 1.15 %) in all four runs and S–S (mean value of 1.29 %, 0.34 %, 1.30 % and 1.85) in runs 1, 2 and 4 (Fig. 7).

In summary, gyral regions as well as gyro-gyral connections consistently involve more than sulcal regions and sulco-sulcal connections within and among the auditory, visual, emotional, and cognitive control functional brain networks during the movie-watching naturalistic stimulus. These findings are consistent with previous studies demonstrating the functional difference between gyri and sulci under resting or task-evoked state based on resting state or task fMRI data [2,14,17,55]. That is, gyri serve as global functional information exchange hubs, and sulci serve as local functional information processing units [2]. The fundamental functional difference between gyri and sulci exists in all of the three states, i. e, resting state, task-evoked, and naturalistic stimulus, during cognitive processing.

Table 2
Comparison of percentage of connections among G-G, G-S and S–S using one-way ANOVA in each of the four runs.

Runs	Mean percentage of connections (%)			One-way ANOVA	
	G-G	G-S	S–S	F-value	P-value
Run 1	2.64	1.49	1.29	8.823	**0.00037**
Run 2	0.85	0.60	0.34	7.719	**0.00092**
Run 3	1.36	0.79	1.30	0.629	**0.03129**
Run 4	2.12	1.15	1.85	5.450	**0.00625**

4. Conclusions

In this study, the functional connectivity characteristics as well as such functional connectivity difference between gyri and sulci during movie-watching naturalistic stimulus are investigated. To the best of our knowledge, this is one of the earliest studies to systematically explore the functional connectivity characteristics difference between gyri and sulci under naturalistic stimulus. A total number of 174 subjects with four different runs of movie-watching naturalistic stimulus as well as resting state 7T fMRI data from the publicly available Human Connectome Project dataset are effectively modeled via the spatio-temporal graph convolutional network model.

Firstly, the experimental results demonstrate that the proposed framework effectively identifies unique functional connectivity features under naturalistic stimulus and achieves the highest classification performance with 93.06 % averaged accuracy, 93.75 % averaged sensitivity, 92.39 % averaged specificity and 93.10 % averaged F1 score compared to other models. Secondly, although the identified unique functional connectivity features vary across the four different runs of movie-watching stimulus, they still exhibit regularity in terms of functional interactions both within and among auditory, visual, emotional,

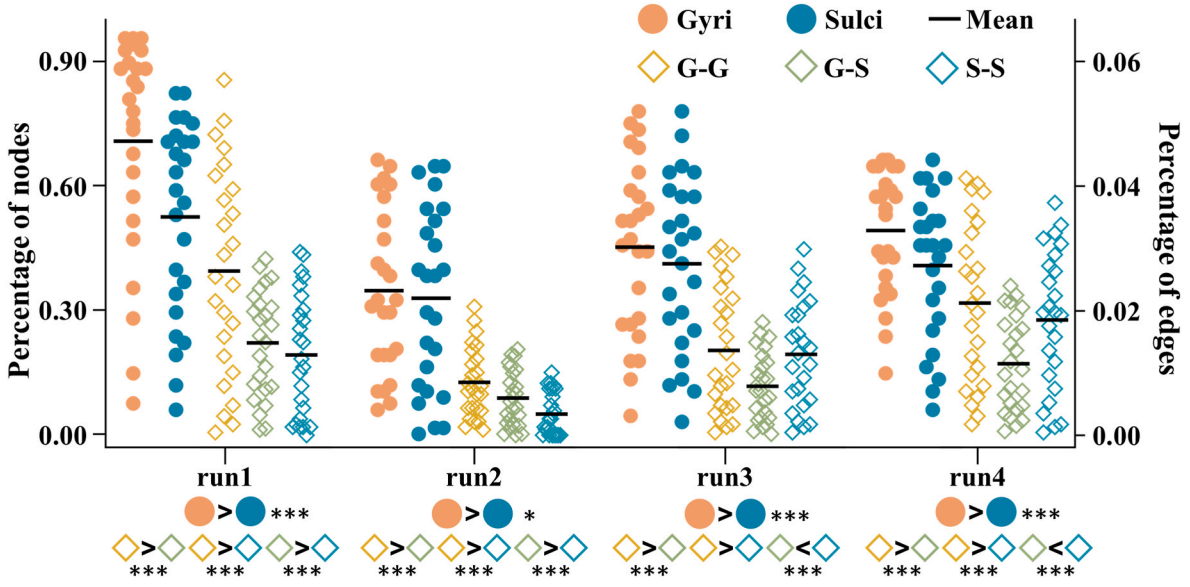

Fig. 7. Statistical comparisons of the percentage of involved numbers of nodes and connections (edges) between gyri and sulci when k ranges from 0.2 % to 5 % (0.2 % as the interval) in each of the four runs. The orange and blue spheres represent the percentage of number of gyral and sulcal regions, respectively. The gold, green and cyan diamonds represent G-G (gyro-gyral), G-S (gyro-sulcal), and S–S (sulco-sulcal) connections, respectively. * indicates $p < 0.05$, and *** indicates $p < 0.001$.

and cognitive control networks. Finally, within these functional connections among different functional brain networks, gyral regions and gyro-gyral connections consistently participate more than sulcal regions and sulco-sulcal connections, suggesting that the principle of fundamental functional difference between gyri and sulci, i.e., gyri are global functional information exchange hubs and sulci are local functional information processing units, also exists under naturalistic stimulus besides resting state or task-evoked state.

One limitation of this study is that the publicly available 174 subjects with both 7T resting state and movie-watching state fMRI data from the Human Connectome Project (HCP) are used. Compared with other studies using 3T resting state or task evoked state fMRI data, the sample size of 7T data is relatively small. Another limitation is that there is no independent test dataset with both 7T resting state and movie-watching state fMRI data to validate the proposed model.

In conclusion, this study for the first time unveils the fundamental principle of functional difference between gyri and sulci under naturalistic stimulus, further extending previous findings on resting and task-evoked states and together warranting that such principle of gyro-sulcal functional difference is universal across all cognitive processing state, which lays a solid foundation for accurate mapping between brain anatomy and function.

In the future, the regularity and variability of gyro-sulcal functional connectivity characteristics under different types (e.g., horror, comedy, etc.) of movie clips could be further investigated if the relevant data are available. The spatio-temporal dynamics of gyro-sulcal effective connectivity characteristics could also be investigated based on various models such as Dynamic Bayesian Networks [56–58]. It is also interesting in exploring the potential relationship of semantics between the visual representations in the gyro-sulcal functional brain connectivity pattern of the biological neural networks and in various of artificial neural networks [59].

Data availability statement

The raw data is from the Human Connectome Project (HCP) as a public available dataset with approval. The analyzed data as well as the proposed deep learning algorithms will be available with publication from the corresponding author (XJ) on reasonable request (including a research proposal), subject to review.

Declaration of competing interest

The authors declare that they have no known competing financial interests or personal relationships that could have appeared to influence the work reported in this paper.

Acknowledgements

This work was supported by the National Natural Science Foundation of China [grant numbers 62276050, 61976045, 62076205, 31971288, U1801265].

Appendix A. Supplementary data

Supplementary data to this article can be found online at https://doi.org/10.1016/j.compbiomed.2023.107747.

References

[1] D.C.V. Essen, A tension-based theory of morphogenesis and compact wiring in the central nervous system, Nature 385 (6614) (1997) 313–318, https://doi.org/10.1038/385313a0.

[2] X. Jiang, T. Zhang, S. Zhang, K.M. Kendrick, T. Liu, Fundamental functional differences between gyri and sulci: implications for brain function, cognition, and behavior, Psychoradiology 1 (1) (2021) 23–41, https://doi.org/10.1093/psyrad/kkab002.

[3] R. Toro, Y. Burnod, Geometric atlas: modeling the cortex as an organized surface, Neuroimage 20 (3) (2003) 1468–1484, https://doi.org/10.1016/j.neuroimage.2003.07.008.

[4] L.Q. Uddin, K. Supekar, H. Amin, E. Rykhlevskaia, D.A. Nguyen, M.D. Greicius, V. Menon, Dissociable connectivity within human angular gyrus and intraparietal sulcus: evidence from functional and structural connectivity, Cerebr. Cortex 20 (11) (2010) 2636–2646, https://doi.org/10.1093/cercor/bhq011.

[5] F. Deng, X. Jiang, D. Zhu, T. Zhang, K. Li, L. Guo, T. Liu, A functional model of cortical gyri and sulci, Brain Struct. Funct. 219 (4) (2014) 1473–1491, https://doi.org/10.1007/s00429-013-0581-z.

[6] T. Zeng, H. Chen, A. Fakhry, X. Hu, T. Liu, S. Ji, Allen mouse brain atlases reveal different neural connection and gene expression patterns in cerebellum gyri and sulci, Brain Struct. Funct. 220 (5) (2015) 2691–2703, https://doi.org/10.1007/s00429-014-0821-x.

[7] V.A. Magnotta, N.C. Andreasen, S.K. Schultz, G. Harris, T. Cizadlo, D. Heckel, P. Nopoulos, M. Flaum, Quantitative in vivo measurement of gyrification in the human brain: changes associated with aging, Cerebr. Cortex 9 (2) (1999) 151–160, https://doi.org/10.1093/cercor/9.2.151.

[8] M. Holland, S. Budday, A. Goriely, E. Kuhl, Symmetry breaking in wrinkling patterns: gyri are universally thicker than sulci, Phys. Rev. Lett. 121 (22) (2018), https://doi.org/10.1103/PhysRevLett.121.228002.

[9] J. Nie, L. Guo, K. Li, Y. Wang, G. Chen, L. Li, H. Chen, F. Deng, X. Jiang, T. Zhang, L. Huang, C. Faraco, D. Zhang, C. Guo, P.T. Yap, X. Hu, G. Li, J. Lv, Y. Yuan, T. Liu, Axonal fiber terminations concentrate on gyri, Cerebr. Cortex 22 (12) (2012) 2831–2839, https://doi.org/10.1093/cercor/bhr361.

[10] M. Jiang, S. Yang, J. Yan, S. Zhang, H. Liu, L. Zhao, H. Dai, J. Lv, T. Zhang, T. Liu, K.M. Kendrick, X. Jiang, Exploring functional difference between gyri and sulci via region-specific 1D convolutional neural networks, Lect. Notes Comput. Sci. (2020) 250–259, https://doi.org/10.1007/978-3-030-59861-7_26.

[11] H. Liu, S. Zhang, X. Jiang, T. Zhang, H. Huang, F. Ge, L. Zhao, X. Li, X. Hu, J. Han, L. Guo, T. Liu, The cerebral cortex is bisectionally segregated into two fundamentally different functional units of gyri and sulci, Cerebr. Cortex 29 (10) (2019) 4238–4252, https://doi.org/10.1093/cercor/bhy305.

[12] C. Amiez, P. Kostopoulos, A.S. Champod, M. Petrides, Local morphology predicts functional organization of the dorsal premotor region in the human brain, J. Neurosci. 26 (10) (2006) 2724–2731, https://doi.org/10.1523/JNEUROSCI.4739-05.2006.

[13] R.P. Rajarethinam, J.R. DeQuardo, R. Nalepa, R. Tandon, Superior temporal gyrus in schizophrenia: a volumetric magnetic resonance imaging study, Schizophr. Res. 41 (2) (2000) 303–312, https://doi.org/10.1016/s0920-9964(99)00083-3.

[14] M. Jiang, Y. Chen, J. Yan, Z. Xiao, W. Mao, B. Zhao, S. Yang, Z. Zhao, T. Zhang, L. Guo, B. Becker, D. Yao, K.M. Kendrick, X. Jiang, Anatomy-guided spatio-temporal graph convolutional networks (AG-STGCNs) for modeling functional connectivity between gyri and sulci across multiple task domains, in: IEEE Transactions on Neural Networks and Learning Systems, 2022, https://doi.org/10.1109/TNNLS.2022.3194733.

[15] S. Yang, Z. Zhao, H. Cui, T. Zhang, L. Zhao, Z. He, H. Liu, L. Guo, T. Liu, B. Becker, K.M. Kendrick, X. Jiang, Temporal variability of cortical gyral-sulcal resting state functional activity correlates with fluid intelligence, Front. Neural Circ. 13 (2019), https://doi.org/10.3389/fncir.2019.00036.

[16] S. Zhang, H. Liu, H. Huang, Y. Zhao, X. Jiang, B. Bowers, L. Guo, X. Hu, M. Sanchez, T. Liu, Deep learning models unveiled functional difference between cortical gyri and sulci, IEEE (Inst. Electr. Electron. Eng.) Trans. Biomed. Eng. 66 (5) (2019) 1297–1308, https://doi.org/10.1109/TBME.2018.2872726.

[17] T. Zhang, X. Li, X. Jiang, F. Ge, S. Zhang, L. Zhao, H. Liu, Y. Huang, X. Wang, J. Yang, L. Guo, X. Hu, T. Liu, Cortical 3-hinges could serve as hubs in cortico-cortical connective network, Brain Imaging and Behavior 14 (6) (2020) 2512–2529, https://doi.org/10.1007/s11682-019-00204-6.

[18] A. Bartels, S. Zeki, Functional brain mapping during free viewing of natural scenes, Hum. Brain Mapp. 21 (2) (2004) 75–85, https://doi.org/10.1002/hbm.10153.

[19] A. Bartels, S. Zeki, Brain dynamics during natural viewing conditions—a new guide for mapping connectivity in vivo, Neuroimage 24 (2) (2005) 339–349, https://doi.org/10.1016/j.neuroimage.2004.08.044.

[20] Y. Golland, S. Bentin, H. Gelbard, Y. Benjamini, R. Heller, Y. Nir, U. Hasson, R. Malach, Extrinsic and intrinsic systems in the posterior cortex of the human brain revealed during natural sensory stimulation, Cerebr. Cortex 17 (4) (2007) 766–777, https://doi.org/10.1093/cercor/bhk030.

[21] C. Tang, Z. Huang, S. Zhou, Q. Wang, F. Yi, J. Nie, Movie-watching fMRI reveals inter-subject synchrony alteration in functional brain activity in ADHD, 11849 LNCS (2019) 104–111, https://doi.org/10.1007/978-3-030-35817-4_13.

[22] S.B. Eickhoff, M. Milham, T. Vanderwal, Towards clinical applications of movie fMRI, Neuroimage 217 (2020), https://doi.org/10.1016/j.neuroimage.2020.116860.

[23] O. Campbell, T. Vanderwal, A.M. Weber, Fractal-based analysis of fMRI BOLD signal during naturalistic viewing conditions, Front. Physiol. 12 (2022), 809943, https://doi.org/10.3389/fphys.2021.809943.

[24] L. Tian, M. Ye, C. Chen, X. Cao, T. Shen, Consistency of functional connectivity across different movies, Neuroimage 233 (2021), 117926, https://doi.org/10.1016/j.neuroimage.2021.117926.

[25] M. Ye, J. Liu, Y. Guan, H. Ma, L. Tian, Are inter-subject functional correlations consistent across different movies? Brain Imaging and Behavior 17 (1) (2023) 44–53, https://doi.org/10.1007/s11682-022-00740-8.

[26] M. Defferrard, X. Bresson, P. Vandergheynst, Convolutional neural networks on graphs with fast localized spectral filtering, Proceedings of the 30th International Conference on Neural Information Processing Systems (2016) 3844–3852.

[27] S. Gadgil, Q. Zhao, A. Pfefferbaum, E.V. Sullivan, E. Adeli, K.M. Pohl, Spatio-temporal graph convolution for resting-state fMRI analysis, in: A.L. Martel, P. Abolmaesumi, D. Stoyanov, D. Mateus, M.A. Zuluaga, S.K. Zhou, D. Racoceanu, L. Joskowicz (Eds.), Medical Image Computing and Computer Assisted Intervention – MICCAI 2020, vol. 12267, Springer International Publishing, 2020, pp. 528–538, https://doi.org/10.1007/978-3-030-59728-3_52.

[28] S. Yan, Y. Xiong, D. Lin, Spatial Temporal Graph Convolutional Networks for Skeleton-Based Action Recognition, 2018. http://arxiv.org/abs/1801.07455.

[29] B. Yu, H. Yin, Z. Zhu, Spatio-temporal graph convolutional networks: a deep learning framework for traffic forecasting, in: Proceedings of the Twenty-Seventh International Joint Conference on Artificial Intelligence, 2018, pp. 3634–3640, https://doi.org/10.24963/ijcai.2018/505.

[30] D.C. Van Essen, K. Ugurbil, E. Auerbach, D. Barch, T.E.J. Behrens, R. Bucholz, A. Chang, L. Chen, M. Corbetta, S.W. Curtiss, S. Della Penna, D. Feinberg, M. F. Glasser, N. Harel, A.C. Heath, L. Larson-Prior, D. Marcus, G. Michalareas, S. Moeller, E. Yacoub, The Human Connectome Project: a data acquisition perspective, Neuroimage 62 (4) (2012) 2222–2231, https://doi.org/10.1016/j.neuroimage.2012.02.018.

[31] M.F. Glasser, S.N. Sotiropoulos, J.A. Wilson, T.S. Coalson, B. Fischl, J.L. Andersson, J. Xu, S. Jbabdi, M. Webster, J.R. Polimeni, D.C. Van Essen, M. Jenkinson, The minimal preprocessing pipelines for the Human Connectome Project, Neuroimage 80 (2013) 105–124, https://doi.org/10.1016/j.neuroimage.2013.04.127.

[32] R.S. Desikan, F. Ségonne, B. Fischl, B.T. Quinn, B.C. Dickerson, D. Blacker, R. L. Buckner, A.M. Dale, R.P. Maguire, B.T. Hyman, M.S. Albert, R.J. Killiany, An automated labeling system for subdividing the human cerebral cortex on MRI scans into gyral based regions of interest, Neuroimage 31 (3) (2006) 968–980, https://doi.org/10.1016/j.neuroimage.2006.01.021.

[33] M.F. Glasser, S.M. Smith, D.S. Marcus, J.L.R. Andersson, E.J. Auerbach, T.E. J. Behrens, T.S. Coalson, M.P. Harms, M. Jenkinson, S. Moeller, E.C. Robinson, S. N. Sotiropoulos, J. Xu, E. Yacoub, K. Ugurbil, D.C. Van Essen, The Human Connectome Project's neuroimaging approach, Nat. Neurosci. 19 (9) (2016) 1175–1187, https://doi.org/10.1038/nn.4361.

[34] C. Destrieux, B. Fischl, A. Dale, E. Halgren, Automatic parcellation of human cortical gyri and sulci using standard anatomical nomenclature, Neuroimage 53 (1) (2010) 1–15, https://doi.org/10.1016/j.neuroimage.2010.06.010.

[35] A. Fornito, A. Zalesky, E. Bullmore, Front Matter. In *Fundamentals Of Brain Network Analysis*, Elsevier, 2016, https://doi.org/10.1016/B978-0-12-407908-3.09996-9 pp. i–ii.

[36] Sergey Ioffe, Christian Szegedy, Batch normalization: accelerating deep network training by reducing internal covariate shift, in: Francis Bach, David Blei (Eds.), Proceedings of the 32nd International Conference on Machine Learning, vol. 37, 2015, pp. 448–456. PMLR, https://proceedings.mlr.press/v37/ioffe15.html.

[37] V. Nair, G.E. Hinton, Rectified linear units improve restricted Boltzmann machines, in: In Proceedings of the 27th International Conference on Machine Learning, ICML-10, 2010, pp. 807–814.

[38] M. Lin, Q. Chen, S. Yan, Network in network. arXiv preprint arXiv:1312.4400. arXiv, http://arxiv.org/abs/1312.4400, 2013.

[39] K.M. Sunnetci, S. Ulukaya, A. Alkan, Periodontal bone loss detection based on hybrid deep learning and machine learning models with a user-friendly application, Biomed. Signal Process Control 77 (2022), 103844, https://doi.org/10.1016/j.bspc.2022.103844.

[40] D.P. Kingma, J. Ba, Adam: A Method for Stochastic Optimization, 2014 *arXiv preprint* arXiv:1412.6980.

[41] S.A. Tuncer, A. Alkan, A decision support system for detection of the renal cell cancer in the kidney, Measurement 123 (2018) 298–303, https://doi.org/10.1016/j.measurement.2018.04.002.

[42] T.A. Hackett, Information flow in the auditory cortical network, Hear. Res. 271 (1–2) (2011) 133–146, https://doi.org/10.1016/j.heares.2010.01.011.

[43] D. Tomasi, N.D. Volkow, Association between functional connectivity hubs and brain networks, Cerebr. Cortex 21 (9) (2011) 2003–2013, https://doi.org/10.1093/cercor/bhq268.

[44] K.N. Ochsner, S.A. Bunge, J.J. Gross, J.D.E. Gabrieli, Rethinking feelings: an fMRI study of the cognitive regulation of emotion, J. Cognit. Neurosci. 14 (8) (2002) 1215–1229, https://doi.org/10.1162/089892902760807212.

[45] K.L. Phan, T. Wager, S.F. Taylor, I. Liberzon, Functional neuroanatomy of emotion: a meta-analysis of emotion activation studies in PET and fMRI, Neuroimage 16 (2) (2002) 331–348, https://doi.org/10.1006/nimg.2002.1087.

[46] C. Humphries, K. Willard, B. Buchsbaum, G. Hickok, Role of anterior temporal cortex in auditory sentence comprehension: an fMRI study, Neuroreport 12 (8) (2001) 1749–1752, https://doi.org/10.1097/00001756-200106130-00046.

[47] P. Morosan, J. Rademacher, A. Schleicher, K. Amunts, T. Schormann, K. Zilles, Human primary auditory cortex: cytoarchitectonic subdivisions and mapping into a spatial reference system, Neuroimage 13 (4) (2001) 684–701, https://doi.org/10.1006/nimg.2000.0715.

[48] M.A. Howard, I.O. Volkov, R. Mirsky, P.C. Garell, M.D. Noh, M. Granner, H. Damasio, M. Steinschneider, R.A. Reale, J.E. Hind, J.F. Brugge, Auditory cortex on the human posterior superior temporal gyrus, J. Comp. Neurol. 416 (1) (2000) 79–92, https://doi.org/10.1002/(SICI)1096-9861(20000103)416:1<79::AID-CNE6>3.0.CO;2-2.

[49] V.A. Lamme, H. Supèr, H. Spekreijse, Feedforward, horizontal, and feedback processing in the visual cortex, Curr. Opin. Neurobiol. 8 (4) (1998) 529–535, https://doi.org/10.1016/S0959-4388(98)80042-1.

[50] C. Stoeckel, P.M. Gough, K.E. Watkins, J.T. Devlin, Supramarginal gyrus involvement in visual word recognition, Cortex 45 (9) (2009) 1091–1096, https://doi.org/10.1016/j.cortex.2008.12.004.

[51] S. Vanni, T. Tanskanen, M. Seppä, K. Uutela, R. Hari, Coinciding early activation of the human primary visual cortex and anteromedial cuneus, Proc. Natl. Acad. Sci. USA 98 (5) (2001) 2776–2780, https://doi.org/10.1073/pnas.041600898.

[52] M.S. Beauchamp, K.E. Lee, B.D. Argall, A. Martin, Integration of auditory and visual information about objects in superior temporal sulcus, Neuron 41 (5) (2004) 809–823, https://doi.org/10.1016/S0896-6273(04)00070-4.

[53] K. Grill-Spector, R. Malach, The human visual cortex, Annu. Rev. Neurosci. 27 (1) (2004) 649–677, https://doi.org/10.1146/annurev.neuro.27.070203.144220.

[54] L.Q. Uddin, J.T. Kaplan, I. Molnar-Szakacs, E. Zaidel, M. Iacoboni, Self-face recognition activates a frontoparietal "mirror" network in the right hemisphere: an event-related fMRI study, Neuroimage 25 (3) (2005) 926–935, https://doi.org/10.1016/j.neuroimage.2004.12.018.

[55] X. Jiang, T. Liu, X. Li, J. Lv, S. Zhao, S. Zhang, W. Zhang, T. Zhang, J. Han, L. Guo, Temporal dynamics assessment of spatial overlap pattern of functional brain networks reveals novel functional architecture of cerebral cortex, IEEE (Inst. Electr. Electron. Eng.) Trans. Biomed. Eng. 65 (6) (2018) 1183–1192, https://doi.org/10.1109/TBME.2016.2598728.

[56] J.C. Rajapakse, J. Zhou, Learning effective brain connectivity with dynamic Bayesian networks, Neuroimage 37 (3) (2007) 749–760, https://doi.org/10.1016/j.neuroimage.2007.06.003.

[57] J. Li, Z.J. Wang, S.J. Palmer, M.J. McKeown, Dynamic Bayesian network modeling of fMRI: a comparison of group-analysis methods, Neuroimage 41 (2) (2008) 398–407, https://doi.org/10.1016/j.neuroimage.2008.01.068.

[58] J. Burge, T. Lane, H. Link, S. Qiu, V.P. Clark, Discrete dynamic Bayesian network analysis of fMRI data, Hum. Brain Mapp. 30 (1) (2009) 122, https://doi.org/10.1002/hbm.20490.

[59] J. Gao, L. Zhao, T. Zhong, C. Li, Z. He, Y. Wei, T. Zhang, Prediction of cognitive scores by joint use of movie-watching fMRI connectivity and eye tracking via Attention-CensNet, Psychoradiology 3 (2023), https://doi.org/10.1093/psyrad/kkad011.